Origin of magnetoelectric effect in $Co_4Nb_2O_9$ and $Co_4Ta_2O_9$: The lessons learned from the comparison of first-principles-based theoretical models and experimental data

I. V. Solovyev[1,2,*] and T. V. Kolodiazhnyi[1]

[1]*National Institute for Materials Science, 1-1 Namiki, Tsukuba, Ibaraki 305-0044, Japan*

[2]*Department of Theoretical Physics and Applied Mathematics, Ural Federal University, Mira Street 19, 620002 Ekaterinburg, Russia*

(Received 20 June 2016; revised manuscript received 15 August 2016; published 22 September 2016)

We report results of joint experimental and theoretical studies on magnetoelectric (ME) compounds $Co_4Nb_2O_9$ and $Co_4Ta_2O_9$. On the experimental side, we present results of the magnetization and dielectric permittivity measurements in the magnetic field. On the theoretical side, we construct the low-energy Hubbard-type model for the magnetically active Co3*d* bands in the Wannier basis, using the input of the first-principles electronic structure calculations, solve this model in the mean-field Hartree-Fock approximation, and evaluate the electric polarization in terms of the Berry phase theory. Both experimental and theoretical results suggest that $Co_4Ta_2O_9$ is magnetically softer than $Co_4Nb_2O_9$. Therefore, it is reasonable to expect that the antiferromagnetic structure of $Co_4Ta_2O_9$ can be easier deformed by the external magnetic field, yielding larger polarization. This trend is indeed reproduced by our theoretical calculations, but does not seem to be consistent with the experimental behavior of the polarization and dielectric permittivity. Thus, we suggest that there should be a hidden mechanism controlling the ME coupling in these compounds, probably related to the magnetic striction or a spontaneous change of the magnetic structure, which breaks the inversion symmetry. Furthermore, we argue that unlike in other ME systems (e.g., Cr_2O_3), in $Co_4Nb_2O_9$ and $Co_4Ta_2O_9$ there are two crystallographic sublattices, which contribute to the ME effect. These contributions are found to be of the opposite sign and tend to compensate each other. The latter mechanism can be also used to control and reverse the electric polarization in these compounds.

DOI: 10.1103/PhysRevB.94.094427

I. INTRODUCTION

The exploration of magnetoelectric (ME) effect—the phenomenon when the magnetization (electric polarization) can be induced by the external electric (magnetic) field—has attracted a great deal of attention, due to its potential applicability in the new generation of multifunctional electronic devices as well as in the fundamental studies aiming at the search of new microscopic mechanisms of the ME coupling. Recently, the ME phenomenon is considered as a part of the more general paradigm called "multiferroism," where the appearance of spontaneous polarization is associated with some massive (and sometimes highly nontrivial) change of the magnetic structure [1].

The canonical material exhibiting the ME effect is the rhombohedral Cr_2O_3, which was discussed by Dzyaloshinskii almost six decades ago [2]. Particularly, the antiferromagnetic structure realized in Cr_2O_3 is such that the spacial inversion $\hat{I}$ enters the magnetic space group only in the combination with the time reversal $\hat{T}$. Therefore, the application of either electric or magnetic field, which destroys $\hat{I}$ or $\hat{T}$, respectively, will destroy also $\hat{I}\hat{T}$, thus giving rise to the electric polarization and the net magnetization. The symmetry properties of the induced electric polarization depend on other symmetry operations, but the existence of $\hat{I}\hat{T}$ is crucial for understanding the ME effect in Cr_2O_3.

The ME effect of a similar origin has been discovered by Fischer *et al.* [3] in 1972 in a family of $M_4A_2O_9$ materials, where $M =$ Co or Mn and $A =$ Nb or Ta. Like in Cr_2O_3, the magnetic structure of $M_4A_2O_9$ obeys the $\hat{I}\hat{T}$ symmetry, which can be destroyed by either electric or magnetic field. The interest to these materials has been recently revived in a series of papers which have addressed the details of the magnetic structure [4–7] and the ME coupling [7–11].

For instance, with the availability of the single crystals it became possible to locate the easy axis for the magnetic moments [6] and to solve the magnetic structure of $Co_4Nb_2O_9$ in the $C2/c'$ magnetic space group [7] in contrast to the $P\bar{3}'c'1$ magnetic space group originally proposed by Bertaut *et al.* [4]. Furthermore, as reported by Khanh *et al.* [7], ME tensor in $Co_4Nb_2O_9$ shows several off-diagonal components which implies the existence of toroidal moment. The title compounds have been classified as linear magnetoelectrics where an applied electric, E (magnetic, H) field induces magnetization, M (polarization, P) [7,9,10,12].

In this contribution we report both experimental and first-principles analysis of magnetic, dielectric, and ME properties of $Co_4Nb_2O_9$ and $Co_4Ta_2O_9$. Both experimental and first-principles results indicate that the tantalate is magnetically softer than the niobate. In accord with these findings, the first-principles based theoretical models predict that the ME coupling should be larger in the $Co_4Ta_2O_9$ than in the $Co_4Nb_2O_9$. These predictions, however, are not supported by available experimental data that show smaller values of magnetically induced spontaneous electrical polarization in $Co_4Ta_2O_9$, thus suggesting that there should be other mechanisms of the ME coupling, which are not taken into account by our models.

The rest of the paper is organized as follows. In Sec. II we will present our experimental data for the magnetic (Sec. II A) and magnetodielectric (Sec. II B) properties of $Co_4Nb_2O_9$ and $Co_4Ta_2O_9$. Results of theoretical calculations will be discussed in Sec. III. Particularly, in Secs. III C and III D we will present our data, respectively, for the behavior of interatomic exchange interactions and the polarization in the magnetic field. Finally,

*solovyev.igor@nims.go.jp

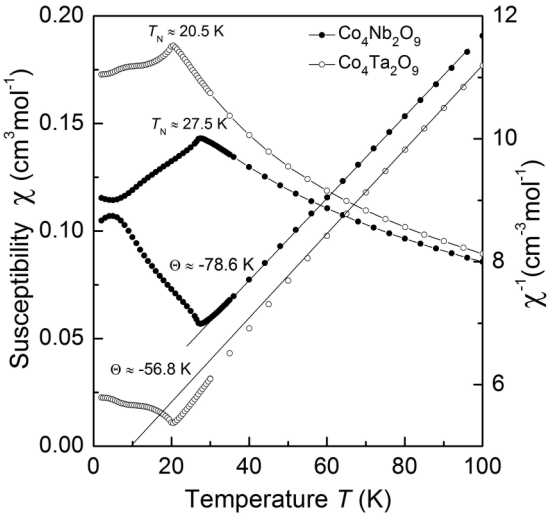

FIG. 1. Temperature dependence of direct and inverse magnetic susceptibilities, χ, and χ^{-1}, respectively, of the $Co_4Nb_2O_9$ and $Co_4Ta_2O_9$ powder samples measured at $H = 50$ Oe. The χ was determined as a ratio of magnetic moment M over magnetic field H.

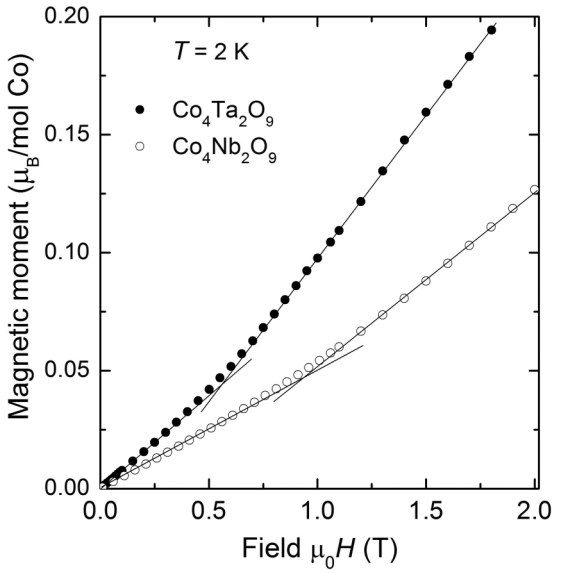

FIG. 2. Field dependence of magnetic moment of Co^{2+} ion in $Co_4Nb_2O_9$ and $Co_4Ta_2O_9$ measured at 2 K.

in Sec. IV we discuss an overall picture emerging from the comparison of experimental and theoretical data and draw our conclusions.

II. MAIN EXPERIMENTAL RESULTS

Sample preparation and measurement details are reported in Ref. [8]. In Sec. II A we will briefly summarize results of our magnetic measurements, which clearly indicate that $Co_4Ta_2O_9$ is magnetically softer than $Co_4Nb_2O_9$. Then, in Sec. II B, we will argue that, as far as the ME properties are concerned, these materials show the opposite tendency and $Co_4Nb_2O_9$ appears to be more responsive to the external magnetic field than $Co_4Ta_2O_9$.

A. Magnetic properties

(i) In accord with the slightly smaller unit cell volume ($V = 326.764(4)$ and $327.737(4)$ Å^3 for $Co_4Nb_2O_9$ and $Co_4Ta_2O_9$, respectively) and in agreement with the literature data [7,9,10], the Néel temperature in $Co_4Nb_2O_9$ ($T_N \approx 27.5$ K) is higher than that in $Co_4Ta_2O_9$ ($T_N \approx 20.5$ K) (Fig. 1). The fit of the inverse magnetic susceptibility to the Curie-Weiss law $\chi(T) = C/(T - \Theta)$ gives a Weiss temperature of $\Theta \approx -78.6$ and -56.8 K and effective magnetic moments of $\mu_{\text{eff}} \approx 5.56\mu_B$ and $5.36\mu_B$ for $Co_4Nb_2O_9$ and $Co_4Ta_2O_9$, respectively. The μ_{eff} are significantly larger than the spin-only effective magnetic moment $\mu_{\text{eff}} = 3.87\mu_B$ for $S = 3/2$, indicating that the orbital angular momentum is not quenched [13].

(ii) Field dependence of the Co^{2+} magnetic moment shows the spin-flop phase transition at $\mu_0 H_c \sim 0.9$ T and ~ 0.5 T for $Co_4Nb_2O_9$ and $Co_4Ta_2O_9$, respectively (Fig. 2). Clearly, $Co_4Ta_2O_9$ is magnetically softer than the $Co_4Nb_2O_9$. Please note that our data on H_c refer to the "average" critical field for polycrystalline materials. They are significantly larger than the $H_c \sim 0.2$ T measured along the easy plane $\mathbf{H} \parallel x$ of the $Co_4Nb_2O_9$ single crystal [7]. The orientation of the crystal is explained in Fig. 3. Note that in our notations x, y, and z correspond to, respectively, $[1\bar{1}0]$, $[\bar{1}\bar{1}0]$, and [001], in the notations of Ref. [7].

B. Magnetodielectric properties

The common problem of multiferroic compounds is a high leakage current and low electrical resistivity due to a relatively narrow band gap and impurity-induced multiple valence states of the transition-metal ions. The title compounds are no exceptions to this rule. Their room temperature resistivities are 3.3×10^5 and 4.4×10^4 Ω cm for $Co_4Nb_2O_9$ and $Co_4Ta_2O_9$, respectively. It is unusual that the tantale shows almost ten times lower resistivity than the niobate, which may be related

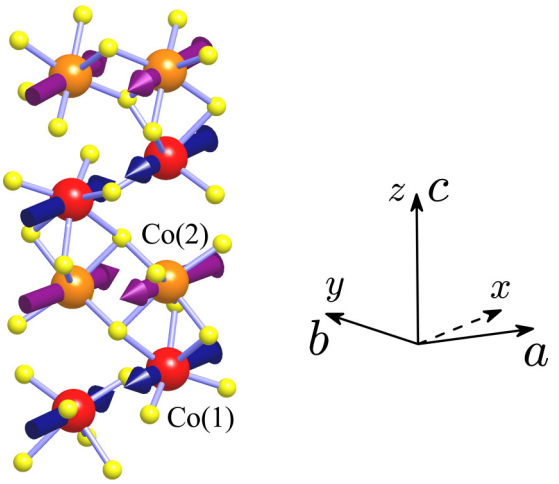

FIG. 3. Fragment of the crystal and magnetic structure of $Co_4Nb_2O_9$ in the ground state. The relative orientation of hexagonal (a, b, and c) and Cartesian (x, y, and z) axes is explained on the right.

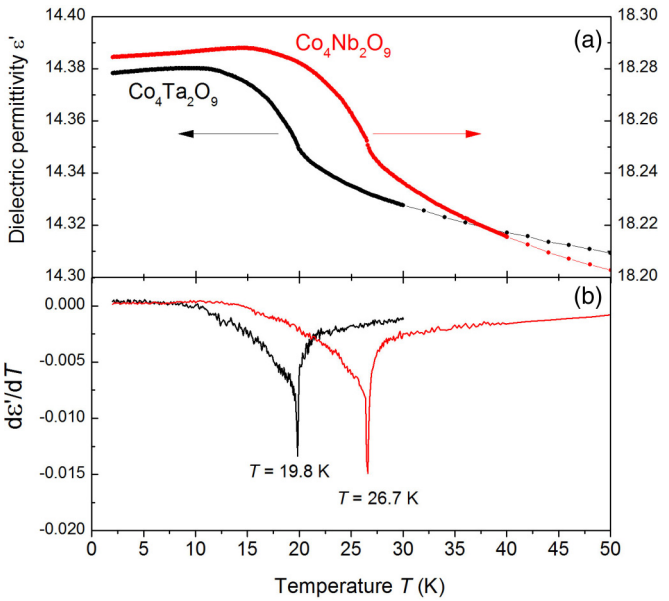

FIG. 4. Zero-field dielectric permittivity (a) and its temperature derivative (b) for $Co_4Nb_2O_9$ and $Co_4Ta_2O_9$ measured at 250 kHz.

to a more narrow band gap of the latter compound (as confirmed by the first-principles calculations discussed in the next section) or to the lower concentration of impurities in the former compound. Zero-field low-temperature dependence of the dielectric permittivity ε' and its first derivative are shown in Fig. 4. The footprint of the antiferromagnetic (AFM) transition is detected as a weak anomaly in the $\varepsilon'(T)$ dependence for both $Co_4Nb_2O_9$ and $Co_4Ta_2O_9$. This indicates a small but finite coupling of the spin ordering to the dielectric response in zero magnetic field which was not reported in the earlier studies [8–10]. This differs from the $MnTiO_3$, a linear magnetoelectric that shows no ME coupling in zero magnetic field [14].

Remarkably, the two title compounds show different magnetocapacitance effect. To better demonstrate this difference we manually subtract the $\varepsilon'(T,H)$ background using the nonlinear interpolation between the ε' end values at ± 1.5 K away from the T_N. The effect of magnetic field on the scaled dielectric permittivity with subtracted background, $\Delta\varepsilon'/H^2$ versus $T - T_N$ is shown in Figs. 5(a) and 5(b). At 1 T, the $\Delta\varepsilon'/H^2$ at $T = T_N$ is ~4 times higher for $Co_4Nb_2O_9$ than for $Co_4Ta_2O_9$. The difference increases to ~88 at magnetic field of 7 T. Clearly, $Co_4Nb_2O_9$ is much more responsive to the magnetic field than the $Co_4Ta_2O_9$ counterpart. Recent literature results also support our conclusions that the niobate shows stronger magnetoelectric response than the tantalate. As revealed by the pyroelectric current measurements of ceramics, the ME coupling constants of $Co_4Nb_2O_9$ and $Co_4Ta_2O_9$ are 18 and 6 ps/m, respectively [9,10].

III. THEORETICAL CALCULATIONS

In order to understand the difference between these two compounds, we turn to the theoretical analysis based on the first-principles electronic structure calculations.

A. Main details of crystal and electronic structure

$Co_4Nb_2O_9$ and $Co_4Ta_2O_9$ crystallize in the centrosymmetric trigonal $P\bar{3}c1$ structure (no. 165). The fragment of this structure is shown in Fig. 3. There are two inequivalent types of Co atoms, alternating along the z axis and forming the (distorted) honeycomb layers in the xy plane. In our electronic structure calculations, we use the experimental

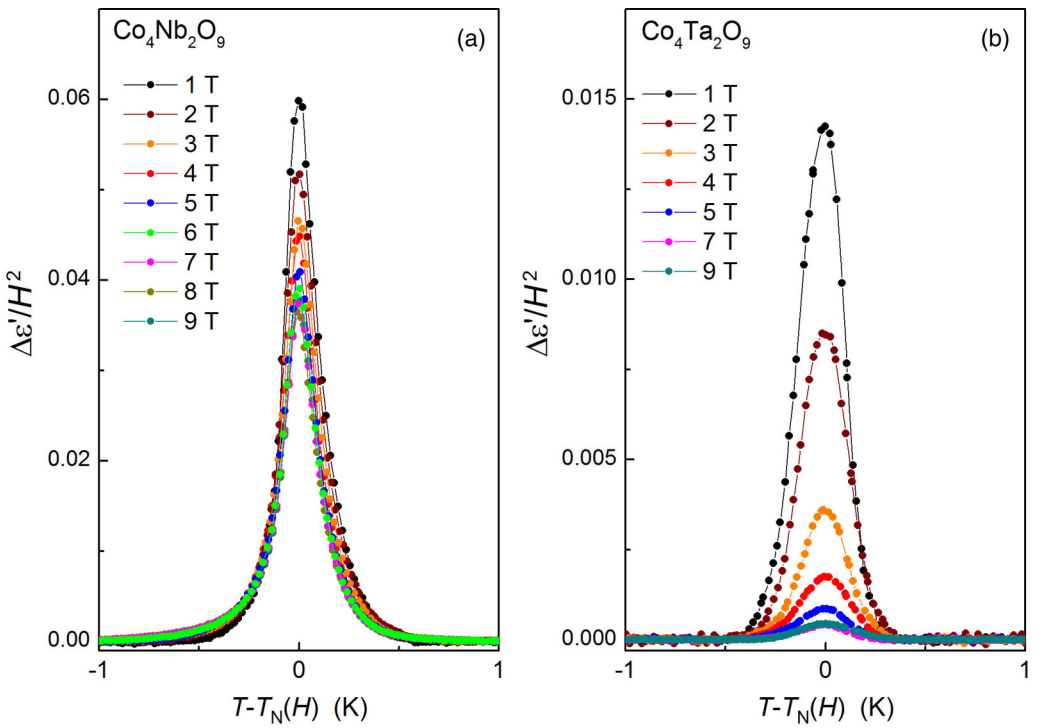

FIG. 5. Scaled dielectric permittivity with subtracted background vs $T - T_N$. Dielectric permittivity was measured at 1 kHz.

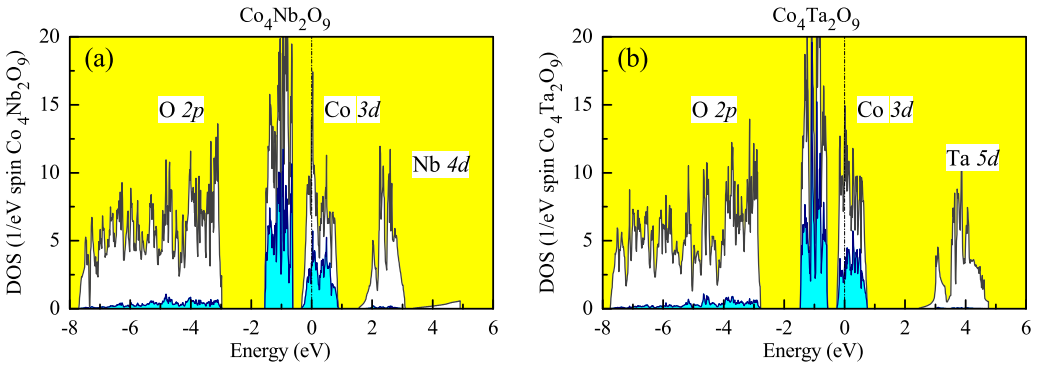

FIG. 6. Total and partial densities of states of $Co_4Nb_2O_9$ and $Co_4Ta_2O_9$ in the local-density approximation. The shaded light (blue) area shows contributions of the Co3d states. Positions of the main bands are indicated by symbols. The Fermi level is at zero energy (shown by dot-dashed line).

room-temperature atomic positions and lattice parameters, reported in Refs. [15,16] for $Co_4Nb_2O_9$ and $Co_4Ta_2O_9$, respectively. All band-structure calculations are based on the linear muffin-tin orbital (LMTO) method in the nearly orthogonal representation (Ref. [17]). All practical details of such calculations (including the choice of atomic sphere, etc.) can be found in Ref. [18]. The total and partial densities of states, obtained in the local-density approximation (LDA), are explained in Fig. 6. The states located near the Fermi level are the Co3d bands, which in the octahedral CoO_6 environment are split into lower-energy t_{2g} and higher-energy e_g bands. These bands are mainly responsible for the magnetic properties of $Co_4Nb_2O_9$ and $Co_4Ta_2O_9$. Regarding the LDA band structure, there are two main differences between $Co_4Nb_2O_9$ and $Co_4Ta_2O_9$. The Ta5d states are considerably more extended in comparison with the Nb4d ones and therefore much stronger hybridize with the O2p states. This explains the additional upward shift of the antibonding Ta5d band, arising from the O2p-Ta5d hybridization. On the other hand, larger unit-cell volume reduces the hybridization and slightly decreases the width of the Co3d bands in $Co_4Ta_2O_9$. In this sense, the Co3d states in $Co_4Ta_2O_9$ are slightly more "localized" in comparison with $Co_4Nb_2O_9$.

B. Effective low-energy electron model

In this section, we briefly remind the reader the main steps of the construction and solution of the effective low-energy model, which is used for the analysis of electronic and magnetic properties of $Co_4Nb_2O_9$ and $Co_4Ta_2O_9$.

The first step of our approach is the construction of the effective Hubbard-type model,

$$\hat{\mathcal{H}} = \sum_{ij}\sum_{\sigma\sigma'}\sum_{ab}\left(t^{ij}_{ab}\delta_{\sigma\sigma'} + \Delta t^{i\sigma\sigma'}_{ab}\delta_{ij}\right)\hat{c}^{\dagger}_{ia\sigma}\hat{c}_{jb\sigma'} + \frac{1}{2}\sum_{i}\sum_{\sigma\sigma'}\sum_{abcd}U^{i}_{abcd}\hat{c}^{\dagger}_{ia\sigma}\hat{c}^{\dagger}_{ic\sigma'}\hat{c}_{ib\sigma}\hat{c}_{id\sigma'}, \quad (1)$$

for the magnetically active Co3d bands, located near the Fermi level, and starting from the electronic band structure in LDA. The corresponding target bands lie in the interval $[-2;1]$ eV in Fig. 6. The model itself is formulated in the basis of Wannier functions, which were constructed for these Co3d bands using the projector-operator technique (Refs. [19,20]) and the orthonormal LMTO's (Ref. [17]) as the trial wave functions. $\sigma(\sigma') = \uparrow$ or $\downarrow$ in (1) are the spin indices, while a, b, c, and d label five 3d orbitals. The parameters of the one-electron part, $\hat{t} = [t^{ij}_{ab}]$, are defined as the matrix elements of the LDA Hamiltonian in the Wannier basis [19]. $\Delta\hat{t} = [\Delta t^{i\sigma\sigma'}_{ab}]$ is the matrix of spin-orbit (SO) interaction, also in the Wannier basis. The parameters of the one-electron Hamiltonian were first computed in the reciprocal (**k**) space and then Fourier transformed to the real space using the grid of $18 \times 18 \times 6$ **k** points in the hexagonal Brillouin zone. Such a grid allows us to calculate the transfer integrals spreading around each Co site up to 20 Å, where all of them practically vanish.

The parameters of screened on-site Coulomb interactions, $\hat{U} = [U^{i}_{abcd}]$, are calculated in the framework of constrained random-phase approximation (RPA) [21], using the simplified procedure, which was explained in Ref. [19].

The crystal-field splitting, obtained from the diagonalization of the site-diagonal part of $\hat{t}$, is shown in Fig. 7. One can clearly see that the main effect is the t_{2g}-e_g splitting in the octahedral CoO_6 environment. Other splittings are considerably smaller. For instance, three t_{2g} levels are split into lower-energy doublet (e'_g) and higher-energy singlet (a_{1g}), being consistent with the d^7 configuration of Co^{2+}, where two minority-spin electrons are accommodated in the lower-energy doublet. The largest splitting of the t_{2g} levels is about 50 meV,

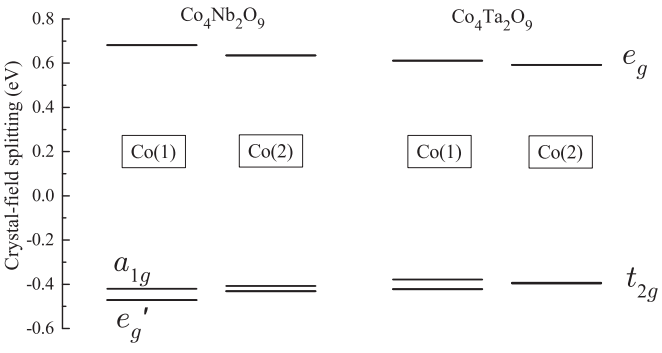

FIG. 7. Scheme of the crystal-field splitting for two inequivalent Co sites in $Co_4Nb_2O_9$ and $Co_4Ta_2O_9$.

TABLE I. Parameters of screened Coulomb interaction (U), exchange interaction (J), and nonsphericity (B) for the inequivalent Co sites in $Co_4Nb_2O_9$ and $Co_4Ta_2O_9$ (in eV).

	$Co_4Nb_2O_9$		$Co_4Ta_2O_9$	
	Co(1)	Co(2)	Co(1)	Co(2)
U	2.95	3.00	3.00	3.29
J	0.94	0.93	0.94	0.95
B	0.10	0.10	0.10	0.10

which is comparable with the strength of the SO coupling ξ (about 75 meV). Thus, one can expect the existence of unquenched orbital magnetization, which is consistent with the experimental susceptibility data.

Each $5\times5\times5\times5$ matrix $\hat{U}=[U^i_{abcd}]$ can be parametrized in terms of three parameters: the Coulomb repulsion $U = F^0$, the intra-atomic exchange interaction $J = (F^2 + F^4)/14$, and the "nonsphericity" $B = (9F^2 - 5F^4)/441$, where F^0, F^2, and F^4 are the screened radial Slater's integrals. The results of such parametrization are shown in Table I. The parameters U are generally larger in $Co_4Ta_2O_9$. This is due to the additional energy separation between the Co3d and Ta5d bands (see Fig. 6), which results in less efficient screening of the Coulomb interactions in the Co3d band by the Ta5d band [19]. Moreover, due to different crystallographic environment, the Coulomb U is different for the Co sites 1 and 2, and this difference is substantially larger in $Co_4Ta_2O_9$. Other parameters of the model Hamiltonian can be found elsewhere [22].

The low-energy model has some limitations, especially for the late transition-metal oxides, which are believed to be close to the charge-transfer regime [23]. Therefore, the O2p states, which are not explicitly considered by our model, may have a significant contribution to the interatomic exchange interactions as well as to the ME effect. The alternative solution is to consider a larger model, in the Wannier basis spanning both Co3d and O2p bands (see Fig. 6), or to use full scale DFT + U calculations (where "DFT" stands for the density functional theory and "+U" is the semiempirical correction for the on-site Coulomb interactions, treating at the mean-field level) [24]. This approach could cure some of the problems of the low-energy model implemented in our work. However, we would also like to caution from exaggerating the abilities of the DFT + U method. Besides the well-known issues related to the choice of parameters of the on-site Coulomb interactions, which is typically fixed in an empirical way, the DFT + U approach relies on some approximate form of the double counting correction, controlling the relative positions of the transition-metal 3d and O2p states. Thus, although DFT + U formally allows us to take into account the contributions of the O2p states, it does it in the very approximate and sometimes uncontrollable way [25]. For multiferroic systems, DFT + U can also lead to wrong directions of noncentrosymmetric atomic displacements, which are inconsistent with the experimental data [26]. This problem of DFT + U does not have a proper solution. Therefore, we believe that it is important to develop an alternative strategy: first, to solve the low-energy model, taking into account rigorously the effect of on-site Coulomb interactions, and then to consider the response of other states in the framework of DFT. The first progress along this line can be found in Ref. [27]. Finally, since the low-energy model is light, it allows us to fully relax the magnetic structure and determine the noncollinear magnetic ground state of $Co_4Nb_2O_9$ and $Co_4Ta_2O_9$, depending on the competition of many magnetic interactions in the system. Similar calculations in DFT + U are much more heavy and typically supplemented with additional constraints imposed on the directions of magnetic moments.

C. Magnetic interactions and magnetic ground state

After the construction, the model was solved in the mean-field Hartree-Fock approximation [19]. Then, the isotropic exchange interactions can be evaluated by considering the infinitesimal rotations of spins and mapping corresponding energy changes onto the spin Heisenberg model $E_H = -\sum_{i>j} J_j \boldsymbol{e}_i \cdot \boldsymbol{e}_{i+j}$, where $\boldsymbol{e}_i$ denotes the *direction of spin* at the site i [28].

We have found that the lowest energy corresponds to the AFM ground state, where all the spins are coupled ferromagnetically along the z axis and antiferromagnetically in the xy plane (see Fig. 3), being in total agreement with the experimental data [7,9]. The corresponding electronic structure is shown in Fig. 8. The 3d states in $Co_4Nb_2O_9$ and $Co_4Ta_2O_9$ are indeed well localized: the atomic levels are split by large crystal field and on-site Coulomb interactions. The interatomic transfer integrals are considerably weaker and lead to the formation of narrow bands around each group of atomic levels. The main difference between $Co_4Nb_2O_9$ and $Co_4Ta_2O_9$ is the additional upward shift of the Co(2) states in the latter compound due to larger Coulomb repulsion (see Table I). In particular, it reduces the band gap in $Co_4Ta_2O_9$, which is formed between minority-spin states of the atoms Co(2) and Co(1). The smaller band gap is consistent with smaller resistivity observed in $Co_4Ta_2O_9$, as reported in Sec. II B.

The obtained type of the magnetic ground state can be easily understood by considering the behavior of interatomic exchange interactions (Fig. 9). One can see that the main interactions are AFM. Partly, this is an artifact of our model analysis, because it does not take into account the polarization of the O2p states, which gives rise to ferromagnetic (FM) contributions to the exchange coupling. For instance, the Néel temperature, estimated using the calculated parameters, is about 170 and 100 K for $Co_4Nb_2O_9$ and $Co_4Ta_2O_9$, respectively. It is strongly overestimated in comparison with the experimental data (27.5 and 20.5 K for $Co_4Nb_2O_9$ and $Co_4Ta_2O_9$, respectively). This overestimation is partly caused by the mean-field approximation. However, there is also an intrinsic error, inherent to the low-energy model itself, because it does not take into account the FM contributions caused by the polarization of the O2p states. Similar overestimation has been found for the Weiss temperature (-255 and -155 K, for $Co_4Nb_2O_9$ and $Co_4Ta_2O_9$, respectively). We would like to note that this problem is not new and was also encountered in other systems, which are close to the charge-transfer regime and where the oxygen states play a more important role [27,29]. The correct quantitative description is possible by considering the direct exchange interactions and the magnetic polarization

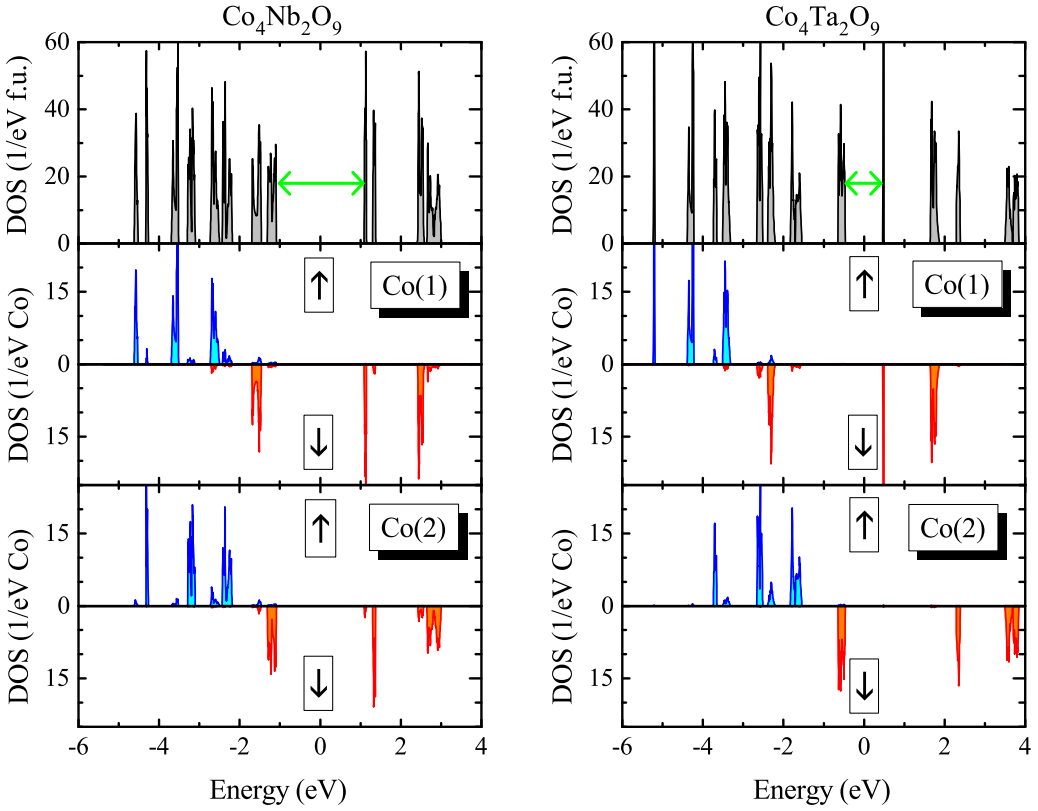

FIG. 8. Total and partial densities of states for the two inequivalent Co sites in $Co_4Nb_2O_9$ and $Co_4Ta_2O_9$, as obtained in the model Hartree-Fock calculations for the antiferromagnetic ground state. The green arrows show the band gap, which is formed between states of the inequivalent Co atoms. The Fermi level is at zero energy.

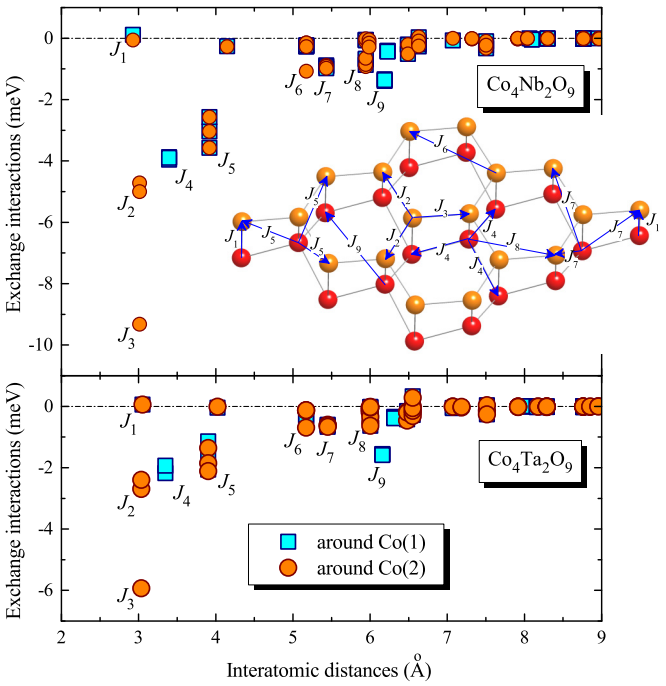

FIG. 9. Distance dependence of interatomic exchange interactions in $Co_4Nb_2O_9$ and $Co_4Ta_2O_9$ around two inequivalent types of Co atoms. The main exchange interactions are explained in the inset, where the Co atoms of the first and second types are shown by darker (red) and lighter (orange) spheres, respectively.

of the O2p band [27]. Nevertheless, at the qualitative level, the magnetic interactions, obtained in the present low-energy model, are consistent with the observed AFM ground state: the main interactions, stabilizing the AFM alignment in the xy plane, are J_2, J_3, and J_4. In the combination with the AFM interaction J_5, they also stabilize the FM alignment along z. The AFM interactions are systematically weaker in $Co_4Ta_2O_9$ (and, therefore, magnetically this system is expected to be softer). This is consistent with somewhat narrower Co3d bandwidth (Fig. 6), larger values of U, which weakens the superexchange interactions, and also smaller band gap between the minority-spin states, which enlarges the FM contributions to the superexchange coupling [30].

After turning on the SO coupling, the magnetic moments become aligned mainly in the xy plane. In this case, we have found two nearly degenerate solutions with the magnetic moments being mainly parallel to either x or y axes and obeying the following symmetries (the magnetic space groups), respectively: $\boldsymbol{G}_1 = \{\hat{E}, \hat{T}\hat{I}, \hat{T}\hat{m}_y, \hat{C}_y^2\}$ (or $C2/c'$ in the notations of Ref. [7]) and $\boldsymbol{G}_2 = \{\hat{E}, \hat{T}\hat{I}, \hat{m}_y, \hat{T}\hat{C}_y^2\}$, where $\hat{E}$ is the unity operation, $\hat{I}$ is the inversion, $\hat{m}_y$ and $\hat{C}_y^2$ are, respectively, the mirror reflection and the 180° rotation about the y axis, combined with the half of the hexagonal translation, $\boldsymbol{c}/2$, and $\hat{T}$ is the time inversion operation. The threefold rotation about the z (c) axis, which is the symmetry operation of the parent space group $P\bar{3}c1$, is forbidden by the magnetic alignment in the xy plane. The first such solution is illustrated in Fig. 3. Both in $\boldsymbol{G}_1$ and $\boldsymbol{G}_2$, the magnetic moments exhibit the

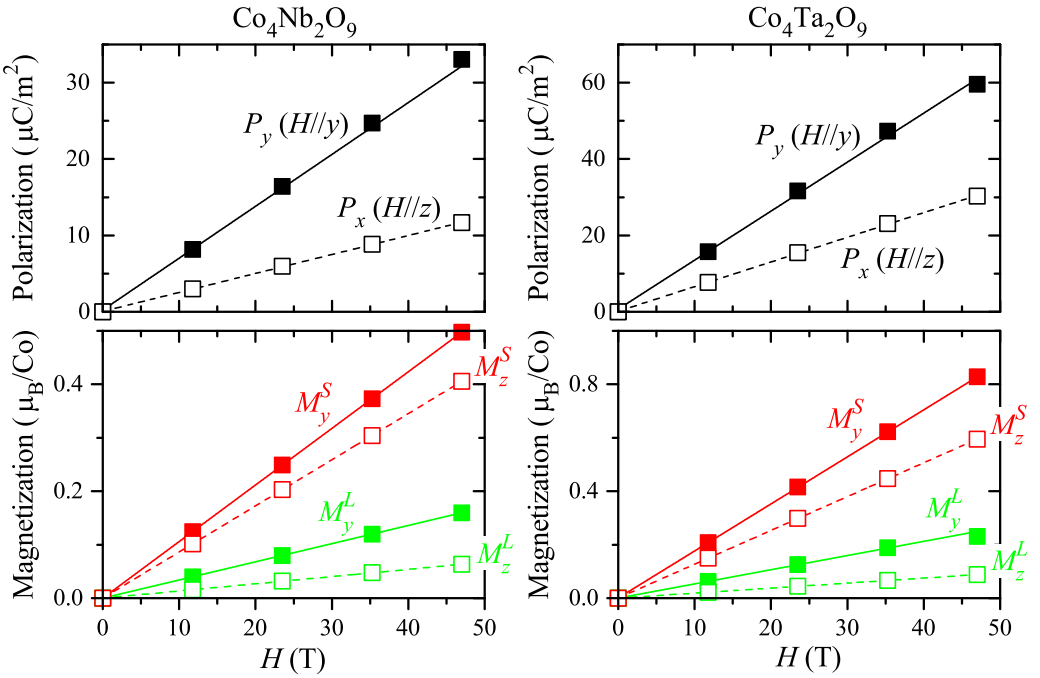

FIG. 10. Nonvanishing components of electric polarization (P) and the net spin (M^S) and orbital (M^L) magnetization as obtained in the model Hartree-Fock calculations for the $\boldsymbol{G}_1$ state in the magnetic field being parallel to either y or z axes.

AFM canting out of the main (either x or y) axis due to the joint effect of the single-ion anisotropy and Dzyaloshinskii-Moriya interactions. The canting angle at the site Co(1) and Co(2) in $Co_4Nb_2O_9$ ($Co_4Ta_2O_9$) is about 2° (1°) and 6° (7°), respectively. This canting is considerably smaller than the experimental one [7], due to the overestimation of isotropic exchange interactions in our low-energy model, which makes these magnetic materials substantially harder than in the experiment. Moreover, we have found an appreciable orbital contribution, which constitutes about 17–20% of the total magnetization at the Co site in the ground state.

D. Magnetic-field dependence of electric polarization

The electronic polarization in the external magnetic field can be computed in the reciprocal space, using the discretized version of the formula of King-Smith and Vanderbilt [31]:

$$\mathbf{P} = -\frac{ie}{(2\pi)^3}\sum_n \int_{BZ} d\mathbf{k}\,\langle u_{n\mathbf{k}}|\partial_{\mathbf{k}} u_{n\mathbf{k}}\rangle, \qquad (2)$$

where $u_{n\mathbf{k}}(\mathbf{r}) = e^{-i\mathbf{kr}}\psi_{n\mathbf{k}}(\mathbf{r})$ is the cell-periodic eigenstate of the model Hamiltonian $H_{\mathbf{k}} = e^{-i\mathbf{kr}} H e^{i\mathbf{kr}}$, which in our case is treated in the Hartree-Fock (HF) approximation, the summation runs over the occupied bands (n), the $\mathbf{k}$-space integration goes over the first Brillouin zone (BZ), and $-e$ ($e > 0$) is the electron charge. In practical calculations we used the grid of $26 \times 26 \times 8$ $\mathbf{k}$ points in the hexagonal Brillouin zone. Other technical details can be found in Ref. [26]. Since the Co3d states in $Co_4Nb_2O_9$ and $Co_4Ta_2O_9$ are well localized (see Fig. 8), the analysis can be also performed in the real space, starting from the limit of atoms states and using the perturbation theory expansion with respect to the transfer integrals [32].

Since $\hat{T}\hat{I}$ is one of the symmetry operations in $\boldsymbol{G}_1$ and $\boldsymbol{G}_2$, these states develop neither spontaneous polarization $\mathbf{P}$ nor the net magnetization $\mathbf{M}$. However, both polarization and magnetization can be induced by the magnetic field, which breaks $\hat{T}\hat{I}$ [2]. The effect of magnetic field was simulated by adding to the model Hamiltonian the term $-\mu_B(2\hat{\boldsymbol{S}} + \hat{\boldsymbol{L}})\mathbf{H}$ at each Co site, where $\hat{\boldsymbol{S}}$ and $\hat{\boldsymbol{L}}$ are, respectively, the spin and orbital angular momentum operators. Thus, we consider both spin and orbital contributions to the ME coupling. Particularly, the orbital contribution was shown to be very important in the systems with unquenched orbital magnetization [33], i.e., similar to $Co_4Nb_2O_9$ and $Co_4Ta_2O_9$. The more rigorous approach to the ME coupling is based on the modern theory of the orbital magnetization [34], which takes into account the on-site as well as some "itinerant" contributions. However, for regular insulating transition-metal oxides, the latter contribution is expected to be small (at least, as long as we are interested in the $\mathbf{k}$-integrated properties) [35]. Therefore, for the purposes of the present work, it is sufficient to consider only the on-site contributions to the orbital magnetization. A similar strategy was also used in Ref. [33].

In the $\boldsymbol{G}_1$ state, there are three possible scenarios. When the magnetic field is applied along the x axis, it causes the spin-flop transition to the $\boldsymbol{G}_2$ state. The magnetic field along the y axis breaks the $\hat{T}\hat{m}_y$ symmetry (while the symmetry operation $\hat{C}_y^2$ remains) and induces the polarization parallel to the y axis. Finally, the magnetic field along the z axis breaks the $\hat{C}_y^2$ symmetry (while $\hat{T}\hat{m}_y$ remains) and induces the polarization in the zx plane. Moreover, we have found that the z component of the electric polarization is negligibly small, which is consistent with the experimental data [7]. The results of such numerical simulations are shown in Fig. 10. In the $\boldsymbol{G}_2$ state, the magnetic field applied along either the x or z axis breaks the $\hat{m}_y$ symmetry (while the symmetry operation $\hat{T}\hat{C}_y^2$

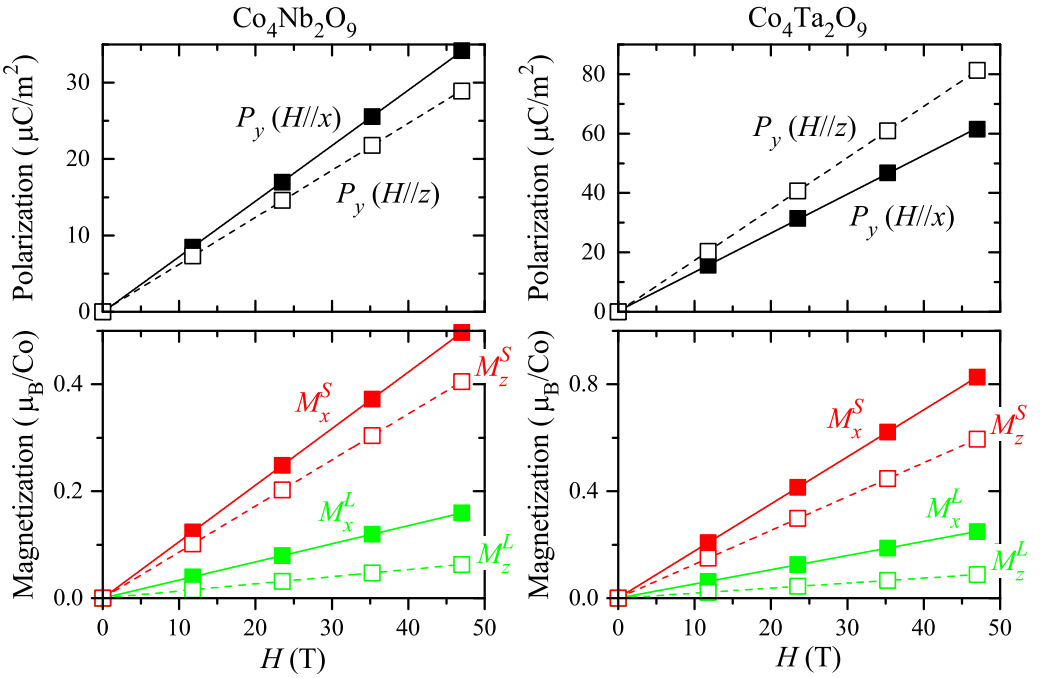

FIG. 11. Nonvanishing components of electric polarization (P) and the net spin (M^S) and orbital (M^L) magnetization as obtained in the model Hartree-Fock calculations for the $\boldsymbol{G}_2$ state in the magnetic field being parallel to either x or z axis.

remains) and induces the electric polarization parallel to the y axis (Fig. 11). The magnetic field along the y axis causes the spin-flop transition to the $\boldsymbol{G}_1$ state. The toroidal moment $\mathbf{T} \sim (\mathbf{P} \times \mathbf{M})$ is expected in the $\boldsymbol{G}_1$ state when $\mathbf{H} \parallel z$ and in the $\boldsymbol{G}_2$ state when $\mathbf{H} \parallel x$ or z [7].

The calculated polarization is generally larger in $Co_4Ta_2O_9$. This is because of two factors. On the one hand, $Co_4Ta_2O_9$ is magnetically softer than $Co_4Nb_2O_9$ and, therefore, the magnetic structure of $Co_4Ta_2O_9$ can be easier deformed by the magnetic field. This effect alone nicely explains the behavior of the electric polarization, when the magnetic field is applied in the xy plane: the dependence of P_y on the total (spin plus orbital) net magnetization is practically identical for $Co_4Nb_2O_9$ and $Co_4Ta_2O_9$ (see Fig. 12). Therefore, for a given magnetic field H, P_y is larger in $Co_4Ta_2O_9$ only because this field induces larger net magnetization. Another factor, which further increases P_x and P_y (for $\boldsymbol{G}_1$ and $\boldsymbol{G}_2$, respectively) in the case of $Co_4Ta_2O_9$, is the smaller band gap (see Fig. 8). Note that in the atomic limit the electric polarization is inversely proportional to the splitting between the occupied and unoccupied atomic levels [32]. Since the band gap is formed between the states of the atoms Co(1) and Co(2), alternating along the z axis (see Fig. 3), this effect will be more important for $\mathbf{H} \parallel z$.

The polarization, calculated for given values of the magnetic field, is substantially underestimated in comparison with the experimental data. The same holds for the matrix elements of the ME tensor. The latter can be estimated using the data reported in Figs. 10 and 11, which yields (in ps/m): $\alpha_{yy} = 0.7$ (1.3), $\alpha_{xz} = 0.3$ (0.7), $\alpha_{yx} = 0.7$ (1.3), and $\alpha_{yz} = 0.6$ (1.7) for $Co_4Nb_2O_9$ ($Co_4Ta_2O_9$). These values are consistent, by the order of magnitude, with the ones reported for Cr_2O_3 and $LiFePO_4$ [33,34]. Nevertheless, the experimental linear ME coupling constant reported for $Co_4Na_2O_9$ and $Co_4Ta_2O_9$

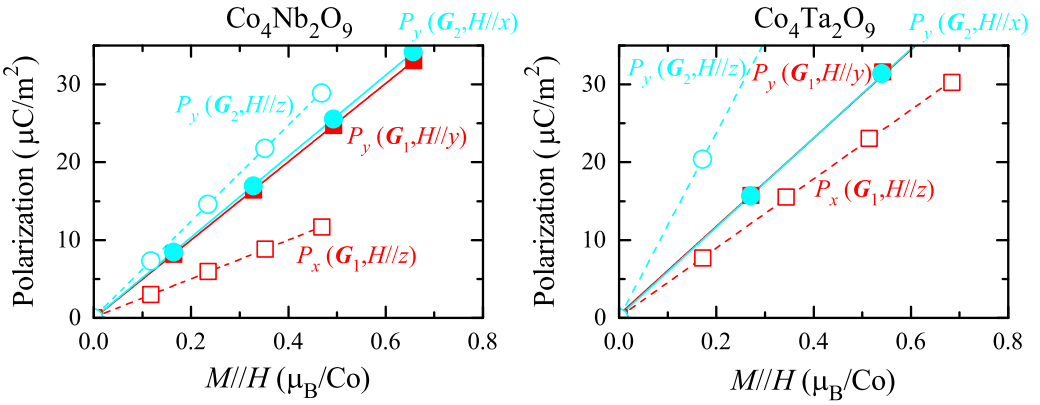

FIG. 12. Electric polarization vs total (spin plus orbital) net magnetization as obtained in the model Hartree-Fock calculations for different directions of the magnetic field in the states $\boldsymbol{G}_1$ and $\boldsymbol{G}_2$.

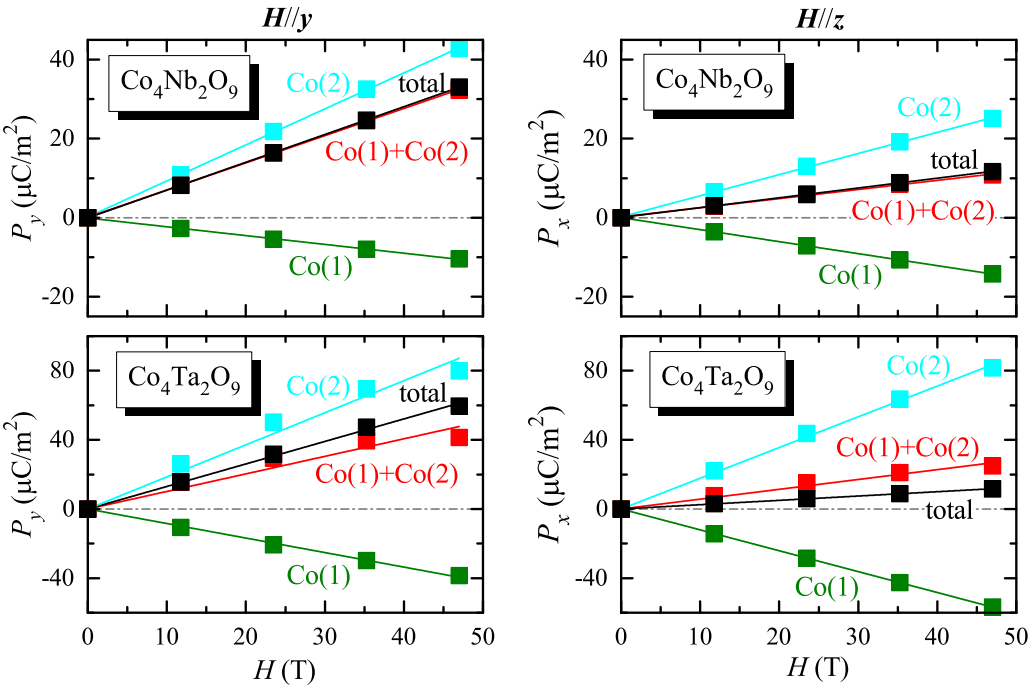

FIG. 13. Electric polarization in $Co_4Nb_2O_9$ and $Co_4Ta_2O_9$ as obtained in the model Hartree-Fock calculations for the $\boldsymbol{G}_1$ state when the magnetic field was applied to either Co(1) or Co(2) sublattice. The sum of these two contributions is denoted as "Co(1)+Co(2)," and "total" is the polarization in the uniform magnetic field applied simultaneously to both magnetic sublattices.

is larger by at least one order of magnitude [7,9,10]. This discrepancy can be explained by the overestimation of the exchange interactions in our low-energy model, which makes the magnetic structure harder than in the experiment. Indeed, if one considers the slope P/M, which is less sensitive to the hardness of the magnetic structure, we will find a much better agreement with the experiment: for instance, for $\mathbf{H} \parallel x$ or y, the theoretical P/M is about 50 $\mu C/(\mu_B m^2)$ both for $Co_4Nb_2O_9$ and $Co_4Ta_2O_9$, which is comparable with the experimental value of about 100 $\mu C/(\mu_B m^2)$ [7,10].

In the $P\bar{3}c1$ structure of $Co_4Nb_2O_9$ and $Co_4Ta_2O_9$, the are two inequivalent sublattices of the Co sites, each of which can exhibit the ME effect: namely, the external magnetic field breaks the inversion symmetry in each of the two sublattices and, therefore, the total polarization is the superposition of such effects in the two sublattices (as well as the interaction between the sublattices). In order to evaluate the contribution of the magnetic inversion symmetry breaking in each of the sublattices, we apply the nonuniform magnetic field, acting on either Co(1) or Co(2) sublattices and evaluate the electric polarization. The results of these calculations for the state $\boldsymbol{G}_1$ are shown in Fig. 13 (the results for the state $\boldsymbol{G}_2$ are very similar and not shown here). The most interesting aspect of these calculations is that the electric polarization induced by the magnetic field in the Co(1) and Co(2) sublattices is of the opposite sign. For $Co_4Nb_2O_9$, the sum of these two contributions is very close to the total polarization, calculated in the uniform magnetic field. The small deviation in the case of $Co_4Ta_2O_9$ is caused by the additional deformation of the magnetic structure in the nonuniform field as well as stronger interublattice interaction due to the smaller band gap (Fig. 8). Thus, we find a strong cancellation of contributions of the two magnetic sublattices to the electric polarization. In the $\boldsymbol{G}_1$ state, this cancellation is especially strong for $\mathbf{H} \parallel z$, which explains the smaller value of the induced polarization than for $\mathbf{H} \parallel y$, in agreement with the experiment [7]. In principle, such an effect offers a possibility to control and reverse the electric polarization.

IV. DISCUSSIONS AND CONCLUSIONS

We have clarified the origin of ME effect in the centrosymmetric trigonal systems $Co_4Nb_2O_9$ and $Co_4Ta_2O_9$. Both compounds form the AFM structure, in which the FM chains of Co atoms are antiferromagnetically coupled in the hexagonal plane. The magnetocrystalline anisotropy tends to align the magnetic moments in the hexagonal plane, thus lowering the original $P\bar{3}c1$ space-group symmetry. Nevertheless, the magnetic alignment obeys the $\hat{I}\hat{T}$ symmetry, meaning that, in the ground state, these compounds exhibit neither net magnetization nor spontaneous polarization, but both of them can be induced by either electric or magnetic field, which breaks $\hat{I}\hat{T}$. In this sense, the situation is similar to the canonical ME compound Cr_2O_3 [2]. The distinct aspect of $Co_4Nb_2O_9$ and $Co_4Ta_2O_9$ is the existence of two inequivalent magnetic sublattices, which contribute to the ME effect. We have found that these contributions are of the opposite signs and, therefore, partly compensate each other. Under certain conditions, this balance can be shifted in either way, thus giving a possibility to control the direction and magnitude of the ME effect.

Summarizing results of our joint experimental and theoretical studies, we first note that, as far as magnetic properties are concerned, $Co_4Ta_2O_9$ seems to be softer than

$Co_4Nb_2O_9$. Experimentally, these tendencies are clearly seen in the behavior of the Néel temperature, the absolute values of the Weiss temperatures, and the critical magnetic field, which causes the spin-flop transition. All these quantities are systematically lower in $Co_4Ta_2O_9$. Moreover, the direct comparison of the behavior of magnetization, which was reported in Refs. [9,10], suggests that the AFM structure can be more easily deformed by the magnetic field to induce larger net magnetization in $Co_4Ta_2O_9$. These experimental data were qualitatively explained by our theoretical calculations of interatomic exchange interactions, which are generally weaker in $Co_4Ta_2O_9$. This behavior in turn nicely correlates with details of the electronic structure calculations of $Co_4Nb_2O_9$ and $Co_4Ta_2O_9$. The quantitative differences between the theory and experiment are related to the fact that the theoretical calculations were performed using minimal effective Hubbard-type model, constructed only for the Co3d bands, which overestimates the tendencies towards antiferromagnetism [27,29].

From the viewpoint of the minimal electron model, considered in the present work, the main factor controlling the behavior of the polarization in $Co_4Nb_2O_9$ and $Co_4Ta_2O_9$ should be the softness of the magnetic structure and its ability to be deformed by the external magnetic field. Then, we would expect that the application of the magnetic field will induce larger polarization in $Co_4Ta_2O_9$ than in $Co_4Nb_2O_9$, as was indeed obtained in our theoretical calculations. However, there are a number of experimental data which suggest the opposite tendency. Particularly the dielectric response to the magnetic field near T_N, studied in the present work, is weaker in $Co_4Ta_2O_9$. Moreover, the experimental polarization, induced for a given magnetic field is systematically smaller in $Co_4Ta_2O_9$ than in $Co_4Nb_2O_9$ [9,10]. Yet the experimental situation is somewhat controversial because direct measurements of the ME susceptibility suggested the opposite tendency [3]: the susceptibility was systematically larger in $Co_4Ta_2O_9$, but exhibited some nonmonotonous behavior as a function of temperature. Moreover, the linear ME coupling constant, reported in Ref. [3], was substantially smaller: about 0.1 and 0.3 ps/m for $Co_4Nb_2O_9$ and $Co_4Ta_2O_9$, respectively. Thus, we believe that this issue requires a more systematic study and it would be important, for instance, to measure directly the ME susceptibility for the single-crystalline sample.

Below, we discuss some factors which have not been taken into account by our theoretical model and which can alter some of our conclusions and also affect the comparison with the experimental data.

(i) The magnetostriction effect in the ordered magnetic phase can play an important role. In our theoretical calculations we used the experimental structure parameters, measured around the room temperature: $T = 297$ K for $Co_4Nb_2O_9$ and $T = 298$ K for $Co_4Ta_2O_9$ [15,16]. These parameters do not take into account some possible change of the crystal structure, which may occur below T_N. Indeed, since the magnetic alignment in the hexagonal plane lowers the original $P\bar{3}c1$ symmetry, it is reasonable to expect also some changes in the crystal structure, which adjust to the change of the magnetic structure. In this sense, it is somewhat surprising that no structural phase transition has been observed so far in the experiment [7]. Nevertheless, some structural change below T_N cannot be completely ruled out because of the following observations. First, the dielectric constant in $Co_4Nb_2O_9$ exhibits a clear upturn below T_N, even without magnetic field, as was observed in Ref. [12] and also confirmed by our measurements. As it was argued in Ref. [12], this change can be of magnetostrictive origin. Second, the electric polarization induced by the magnetic field in $Co_4Nb_2O_9$ has a pronounced off-diagonal component [7]. This finding is inconsistent with the $P\bar{3}c1$ symmetry, according to which the polarization should be parallel to the y axis for $\mathbf{H} \parallel x$ or y (depending on the magnetic state), or parallel to either the y or x axis when $\mathbf{H} \parallel z$, but there should be no off-diagonal components of the polarization in the xy plane.

(ii) The magnetostriction implies that the crystal structure is soft and can be changed by the magnetic realignment. If so, a similar change can be induced by the magnetic field, which breaks the $\hat{I}\hat{T}$ symmetry and, therefore, can shift the atoms from their centrosymmetric positions. This will produce an additional lattice contribution to the polarization and magnetoelectric tensor. The previous theoretical studies on Cr_2O_3 and $LiNiPO_4$ suggested that the lattice contribution can be as large as the electronic one [36]. Moreover, these two contributions can be of the opposite signs, thus providing various scenarios of compensation between them. Unfortunately, the lattice contribution cannot be easily taken into account in the low-energy model, which we consider in the present work and which is constructed for the fixed crystal structure. Nevertheless, this may be an important contribution, which should be carefully considered in future studies and which can substantially revise the behavior of polarization and magnetoelectric tensor in $Co_4Nb_2O_9$ and $Co_4Ta_2O_9$.

(iii) Another important issue is the possible change of the magnetic structure, which can be induced, for instance, by poling electric field used in some of the experiments (e.g., in Ref. [7]) or some other factors. Particularly, how robust is the AFM ground state and whether $Co_4Nb_2O_9$ and $Co_4Ta_2O_9$ are the conventional ME systems, or whether these compounds under certain conditions can become type-II multiferroics, where the onset of electric polarization is triggered by some massive changes in the magnetic structure, which breaks spontaneously the inversion symmetry [1]? The above scenario looks quite feasible taking into account the complexity of magnetic interactions (Fig. 9), many of which are antiferromagnetic, not necessarily restricted by the nearest neighbors, and compete with each other. On many occasions such behavior is responsible for the type-II multiferroism [1,26,37]. In order to explore this possibility in $Co_4Nb_2O_9$ and $Co_4Ta_2O_9$ we have performed self-consistent HF spin-spiral calculations without the SO coupling, based on the generalized Bloch theorem [38]. The results are presented in Fig. 14. In this case, $\boldsymbol{q} = 0$ corresponds to the ground-state AFM alignment, which is deformed for finite spin-spiral propagation vectors $\boldsymbol{q}$. For each value of $\boldsymbol{q}$, the magnetic moments in the xy plane were allowed to freely relax in order to minimize the total energy of the system. For $\boldsymbol{q} \parallel z$ the dependence $E(q)$ is very flat (contrary to $\boldsymbol{q} \parallel x$) when the energy change is within 1 meV/Co even for relatively large $q = |\boldsymbol{q}|$. In such a situation the ground state is still $\boldsymbol{q} = 0$. However, any perturbation of the magnetic system, linear in $\boldsymbol{q}$, can induce the transition to a noncollinear state with the broken inversion symmetry, which will further

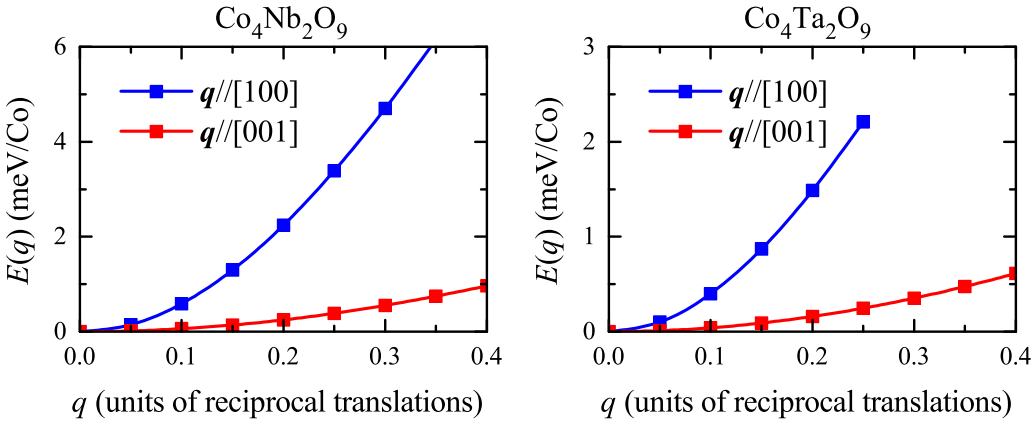

FIG. 14. Dependence of the total energy on the spin-spiral vector q as obtained in the mean-field Hartree-Fock calculations for $Co_4Nb_2O_9$ and $Co_4Ta_2O_9$.

affect the behavior of electric polarization. For instance, such a transition can be caused by the electric field, leading to the off-centrosymmetric atomic displacements and appearance of Dzyaloshinskii-Moriya interactions [39], connecting different unit cells.

ACKNOWLEDGMENTS

The work of I.V.S. was partly supported by a Russian Science Foundation grant (Project No. 14-12-00306). T.V.K. was supported by a Grant-in-Aid for Scientific Research C (Grant No. 26400323) from JSPS.

[1] T. Kimura, Annu. Rev. Mater. Res. **37**, 387 (2007); S.-W. Cheong and M. Mostovoy, Nat. Mater. **6**, 13 (2007); D. Khomskii, Physics **2**, 20 (2009); Y. Tokura and S. Seki, Adv. Mater. **22**, 1554 (2010).

[2] I. E. Dzyaloshinskii, J. Exp. Theor. Phys. **37**, 881 (1959).

[3] E. Fischer, G. Gorodetsky, and R. M. Hornreich, Solid State Commun. **10**, 1127 (1972).

[4] E. F. Bertaut, L. Corliss, F. Forrat, R. Aleonard, and R. Pauthenet, J. Phys. Chem. Solids **21**, 234 (1961).

[5] B. Schwarz, D. Kraft, R. Theissmann, and H. Ehrenberg, J. Magn. Magn. Mater. **322**, L1 (2010).

[6] Y. Cao, Y. Yang, M. Xiang, Z. Feng, B. Kang, J. Zhang, W. Ren, and S. Cao, J. Cryst. Growth **420**, 90 (2015).

[7] N. D. Khanh, N. Abe, H. Sagayama, A. Nakao, T. Hanashima, R. Kiyanagi, Y. Tokunaga, and T. Arima, Phys. Rev. B **93**, 075117 (2016).

[8] T. Kolodiazhnyi, H. Sakurai, and N. Vittayakorn, Appl. Phys. Lett. **99**, 132906 (2011).

[9] Y. Fang, Y. Q. Song, W. P. Zhou, R. Zhao, R. J. Tang, H. Yang, L. Y. Lv, S. G. Yang, D. H. Wang, and Y. W. Du, Sci. Rep. **4**, 3860 (2014).

[10] Y. Fang, S. Yan, L. Zhang, Z. Han, B. Qian, D. Wang, and Y. Du, J. Am. Ceram. Soc. **98**, 2005 (2015).

[11] Y. Fang, W. P. Zhou, S. M. Yan, R. Bai, Z. H. Qian, Q. Y. Xu, D. H. Wang, and Y. W. Du, J. Appl. Phys. **117**, 17B712 (2015).

[12] Y. M. Xie, C. S. Lin, H. Zhang, and W. D. Cheng, AIP Adv. **6**, 045006 (2016).

[13] The effective moments reported here are higher than the $\sim 4.73\mu_B$ expected for Co^{2+} with the maximal possible orbital moment $L = 1$ for the t_{2g} shell, spin moment $S = 3/2$, and total moment $J = 5/2$ [N. W. Ashcroft and N. D. Mermin, *Solid State Physics* (Holt, Rinehart and Winston, Austin, TX, 1976)]. A similar problem was encountered in Ref. [7]. We speculate that the difference can be caused by the magnetic polarization of the O and Nb(Ta) states, which causes some deviation from the Curie-Weiss behavior for the localized spins. This scenario qualitatively explains smaller value of μ_{eff} in $Co_4Ta_2O_9$, which is consistent with weaker polarizability of the Ta5*d* states due to their shift to the higher-energy region (Fig. 6). The deviation from the Curie-Weiss dependence at T as high as 55 K is indeed seen in Fig. 1 for $Co_4Ta_2O_9$ which introduces significant uncertainty in the Θ value. Even larger deviation from the Curie-Weiss dependence was reported in Ref. [7] for $Co_4Nb_2O_9$ single crystal.

[14] N. Mufti, G. R. Blake, M. Mostovoy, S. Riyadi, A. A. Nugroho, and T. T. M. Palstra, Phys. Rev. B **83**, 104416 (2011).

[15] M. A. R. Castellanos, S. Bernès, and M. Vega-González, Acta Crystallogr. Sect. E **62**, i117 (2006).

[16] W. Wong-Ng, H. F. McMurdie, B. Paretzkin, C. R. Hubbard, A. L. Dragoo, and J. M. Stewart, Powder Diffr. **2**, 106 (1987).

[17] O. Gunnarsson, O. Jepsen, and O. K. Andersen, Phys. Rev. B **27**, 7144 (1983).

[18] https://www2.fkf.mpg.de/andersen/LMTODOC.html.

[19] I. V. Solovyev, J. Phys.: Condens. Matter **20**, 293201 (2008).

[20] N. Marzari, A. A. Mostofi, J. R. Yates, I. Souza, and D. Vanderbilt, Rev. Mod. Phys. **84**, 1419 (2012).

[21] F. Aryasetiawan, M. Imada, A. Georges, G. Kotliar, S. Biermann, and A. I. Lichtenstein, Phys. Rev. B **70**, 195104 (2004).

[22] All parameters of the model Hamiltonian are available upon request.

[23] J. Zaanen, G. A. Sawatzky, and J. W. Allen, Phys. Rev. Lett. **55**, 418 (1985).

[24] V. I. Anisimov, J. Zaanen, and O. K. Andersen, Phys. Rev. B **44**, 943 (1991).

[25] I. V. Solovyev and K. Terakura, Phys. Rev. B **58**, 15496 (1998).

[26] I. V. Solovyev, M. V. Valentyuk, and V. V. Mazurenko, Phys. Rev. B **86**, 144406 (2012).
[27] I. V. Solovyev, I. V. Kashin, and V. V. Mazurenko, Phys. Rev. B **92**, 144407 (2015).
[28] A. I. Liechtenstein, M. I. Katsnelson, V. P. Antropov, and V. A. Gubanov, J. Magn. Magn. Matter. **67**, 65 (1987).
[29] I. V. Solovyev, Phys. Rev. B **91**, 224423 (2015).
[30] K. I. Kugel and D. I. Khomskii, Sov. Phys. Usp. **25**, 231 (1982).
[31] R. D. King-Smith and D. Vanderbilt, Phys. Rev. B **47**, 1651 (1993); D. Vanderbilt and R. D. King-Smith, *ibid.* **48**, 4442 (1993); R. Resta, J. Phys.: Condens. Matter **22**, 123201 (2010).
[32] I. V. Solovyev and S. A. Nikolaev, Phys. Rev. B **90**, 184425 (2014).
[33] A. Scaramucci, E. Bousquet, M. Fechner, M. Mostovoy, and N. A. Spaldin, Phys. Rev. Lett. **109**, 197203 (2012).
[34] A. Malashevich, S. Coh, I. Souza, and D. Vanderbilt, Phys. Rev. B **86**, 094430 (2012).
[35] S. A. Nikolaev and I. V. Solovyev, Phys. Rev. B **89**, 064428 (2014).
[36] E. Bousquet, N. A. Spaldin, and K. T. Delaney, Phys. Rev. Lett. **106**, 107202 (2011).
[37] I. V. Solovyev and Z. V. Pchelkina, Phys. Rev. B **82**, 094425 (2010); **90**, 179909(E) (2014); I. V. Solovyev, *ibid.* **83**, 054404 (2011); **90**, 179910(E) (2014).
[38] L. M. Sandratskii, Adv. Phys. **47**, 1 (1998).
[39] I. Dzyaloshinsky, J. Chem. Phys. Solids **4**, 241 (1958); T. Moriya, Phys. Rev. **120**, 91 (1960).